Proc. Natl. Acad. Sci. USA
Vol. 90, pp. 1474–1478, February 1993
Biochemistry

Crystal structure of *Escherichia coli* L-asparaginase, an enzyme used in cancer therapy

(amidohydrolase/leukemia/active site/aspartate)

AMY L. SWAIN, MARIUSZ JASKÓLSKI*, DOMINIQUE HOUSSET†, J. K. MOHANA RAO, AND ALEXANDER WLODAWER‡

Macromolecular Structure Laboratory, National Cancer Institute–Frederick Cancer Research and Development Center, ABL–Basic Research Program, Frederick, MD 21702-1201

Communicated by David R. Davies, October 19, 1992 (received for review July 30, 1992)

ABSTRACT **The crystal structure of *Escherichia coli* asparaginase II (EC 3.5.1.1), a drug (Elspar) used for the treatment of acute lymphoblastic leukemia, has been determined at 2.3 Å resolution by using data from a single heavy atom derivative in combination with molecular replacement. The atomic model was refined to an *R* factor of 0.143. This enzyme, active as a homotetramer with 222 symmetry, belongs to the class of α/β proteins. Each subunit has two domains with unique topological features. On the basis of present structural evidence consistent with previous biochemical studies, we propose locations for the active sites between the N- and C-terminal domains belonging to different subunits and postulate a catalytic role for Thr-89.**

Two isozymes of L-asparaginase (EC 3.5.1.1), which catalyze the hydrolysis of L-asparagine to L-aspartate and ammonia, are produced by *Escherichia coli* (1). Type I *E. coli* asparaginase (EcAI) is located in the cytosol, whereas type II (EcA) is located in the periplasmic region of the bacteria and has a much higher affinity for asparagine (K_m = 11.5 μM) than EcAI (2). Production of EcA is dramatically increased (>100-fold) under anaerobic conditions when amino acids are the primary source of carbon for the bacteria. In this case, asparaginase is likely to participate in the oxaloacetate pathway (3). EcA is active as a tetramer of identical subunits (4), each of 35.6 kDa (5). This enzyme has antileukemic activity and is used clinically for the treatment of acute lymphoblastic leukemia (1, 6).

Much effort has been made to characterize EcA, but has yielded few details about its mode of neoplastic inhibition or its enzymatic mechanism (7). The enzyme is effective against neoplasias that require asparagine and obtain it from circulating pools (8), presumably because the cancer cells have diminished expression of asparagine synthetase (9). It is uncertain, however, whether neoplastic cell death after asparaginase administration results directly from the depletion of circulating asparagine levels or, indirectly, from some other metabolite of the asparaginase reaction (10). Nevertheless, this enzyme has been in clinical use for many years, affecting complete disease remission in some cases, as well as proving effective in maintenance therapy.

Biochemical studies have given little insight into the mechanism of the asparaginase reaction *in vitro*. Substrate-analog modification studies of different but homologous amidohydrolases have given seemingly conflicting results in attempts to identify residues important for activity (12, 13). In one case, the substrate analog was bound to a residue conserved among all bacterial asparaginases, Thr-12, of *Acinetobacter glutaminasificans* glutaminase-asparaginase (AGA) (12) and in another case to Ser-120 of EcA (13), a residue that is not conserved. Chemical modification of the enzyme and ^{1}H NMR spectroscopy indicated that a histidine residue and one or two tyrosine residues may be necessary for activity (14), but subsequent mutagenesis studies indicate that none of the histidine residues in EcA are required for catalysis (15). The most convincing evidence for the location of a residue important for activity comes from a recent report that shows loss of asparaginase activity when Thr-12 is mutated to alanine, but preservation of activity when it is mutated to serine (16).

Crystallographic investigations of asparaginase and related amidohydrolases have been going on for over 20 years (17–22), resulting in a partially correct model of AGA (22) and a very low-resolution map of EcA in which the only recognized structural elements were two long helices (18). In view of the importance of this macromolecule, both as an enzyme and as a drug, and the need to clarify the conflicting biochemical reports, we pursued the study of its structure at high resolution. We report here the x-ray crystallographic structure§ of EcA, determined by using single isomorphous replacement and anomalous scattering data, combined with information from molecular replacement (MR) by using the preliminary model of AGA (22) as a probe.

MATERIALS AND METHODS

Crystallization. EcA was obtained in the form of Elspar concentrate (product 38663, Rx 95885; Merck, Sharp and Dohme). Previously unreported monoclinic crystals were grown in hanging drops from 0.1 M sodium acetate (pH 5) equilibrated against 0.1 M sodium acetate, pH 5/2-methyl-2,4-pentanediol/25% polyethylene glycol 3350, 50:33:17 (vol/vol). The space group is $P2_1$ with unit cell parameters a = 76.7 Å, b = 96.1 Å, c = 111.3 Å, and β = 97.1°, and each asymmetric unit contains a complete tetramer of EcA.

X-Ray Data Collection and Processing. X-ray intensity data were collected using a Siemens area detector mounted on a three-axis goniometer. The native data are 90% complete to 2.5 Å and 74% complete at 2.3 Å, with a redundancy of 5.4. The R_{merge} for data collected from five different crystals is 0.055, where $R_{merge} = \Sigma|I_i - \langle I\rangle|/\Sigma\langle I\rangle$. An isomorphous

The publication costs of this article were defrayed in part by page charge payment. This article must therefore be hereby marked "*advertisement*" in accordance with 18 U.S.C. §1734 solely to indicate this fact.

Abbreviations: EcAI, type I *E. coli* asparaginase; EcA, type II *E. coli* asparaginase; AGA, *Acinetobacter glutaminasificans* glutaminase-asparaginase; ErA, *Erwinia chrysanthemi* asparaginase; MR, molecular replacement.

*Present address and on leave from: A. Mickiewicz University, Faculty of Chemistry, Poznań, Poland.
†Present address: Institut de Biologie Structurale, Laboratoire de Cristallographie et Cristallogénèse des Protéines, Batiment 4, 41, avenue des Martyrs, 38027 Grenoble cedex 1, France.
‡To whom reprint requests should be addressed.

§The atomic coordinates and structure factors have been deposited in the Protein Data Bank, Chemistry Department, Brookhaven National Laboratory, Upton, NY 11973 (reference 2ECA, 2ECASF).

derivative was obtained by soaking a native crystal for 3.5 days in a solution of 10 mM uranyl nitrate in the buffer described above. Derivative data were measured from one crystal, resulting in a set with 24,407 unique reflections and 13,399 Friedel pairs {R_{merge} = 0.061 with a redundancy of 1.7; the anomalous R factor was R_a = 0.085, where $R_a = [\Sigma||F(hkl)| - |F(\overline{hkl})||]/[0.5\Sigma(|F(hkl)| + |F(\overline{hkl})|)]$}. The R_{diff} between native (N) and derivative (D) data in the resolution range of 35–3.5 Å is 0.177, where $R_{diff} = \Sigma|F_N - F_D|/\Sigma F_N$. All calculations were made with $I \geq 1.5\sigma(I)$ data. Other statistics for the heavy atom derivative are given in Table 1.

The only previously published amidohydrolase structure was that of AGA reported by this laboratory at 2.9 Å resolution (22). That model consisted of two polypeptide chains with a total of 331 residues per subunit, and its known shortcomings were identified. In particular, although most of the secondary structure elements were identified correctly, the direction of the chains, as well as the connections between the elements, remained in doubt. This imperfect model was, however, sufficient to locate the EcA tetramer in its unit cell. Several MR techniques were employed for this purpose, all leading to the same solution, and the one used for subsequent analysis was that obtained from X-PLOR (23). A peak of 5σ in the resolution range 8–4 Å with a 0.2° grid was found at θ_1 = 191.8°, θ_2 = 29.2°, and θ_3 = 75.6°. The translation function showed the position of the tetramer to be x = 0.25, z = 0.25 or x = 0.75, z = 0.25 (y was arbitrarily set to 0.0 in the space group $P2_1$).

A difference-Patterson map for the uranyl derivative of EcA revealed numerous Harker peaks that could not be fully deconvoluted. However, an ($F_D - F_N$) difference Fourier map, calculated by using phases from the MR solution based on the AGA model discussed above, had the first 11 peaks substantially above background. A search for difference-Patterson cross vectors between those 11 sites showed that 9 of them represented a self-consistent set, and only these sites were used for subsequent phasing to 3.5 Å. A lack-of-closure refinement carried out in PROTEIN (24) resulted in the heavy atom parameters and statistics shown in Table 1. The single isomorphous replacement/anomalous scattering phases at that stage were the starting point for a solvent flattening procedure carried out by using the programs of Wang (25). The solvent flattening process was continued with stepwise phase extension to 3 Å resolution. This process was carried out in nine steps, adding approximately one reciprocal lattice point per step, which was equivalent to 1200–1400 reflections.

Table 1. Uranyl derivative statistics

Step 1: Heavy atom refinement				
FOM			0.39	
R_{Cullis}			0.599	
Phasing power			1.63	
Resolution, Å			35.0–3.5	
Site	RO	x	y	z
1	1.72	0.317	−0.015	0.117
2	1.69	0.301	0.020	0.110
3	1.56	1.122	−0.089	0.335
4	1.42	1.145	−0.075	0.358
5	1.38	0.783	0.467	0.550
6	1.34	0.784	0.439	0.567
7	1.32	0.807	0.518	−0.018
8	1.05	0.792	0.481	−0.039
9	0.98	1.038	0.512	0.476
Step 2: Solvent flattening				
Solvent content			0.41	
Map inversion R			0.188	
FOM			0.81	
F_o/F_c correlation coefficient			0.977	
Reflections			16,591	
Resolution, Å			35.0–3.5	
Step 3: Phase extension				
Map inversion R			0.179	
FOM			0.73	
F_o/F_c correlation coefficient			0.987	
Reflections			31,036	
Resolution, Å			35.0–3.0	

RO, relative occupancy; *FOM*, figure of merit.

Phases were improved by averaging the electron density maps [using SARASA (J.K.M.R. with modifications by M.J.)] with respect to the three local dyads of the EcA tetramer in the asymmetric part of the unit cell. The transformation matrices defining the 222 molecular symmetry were optimized by maximizing the correlation coefficients between superimposed subunit densities. By using the optimized transformations, the map was averaged in an iterative process until the phase change became negligible and there was no significant increase in density correlation coefficients between subunits. (Over eight cycles the mean phase change decreased from 54.4° to 3.8°, and the final density correlation coefficients between subunits ranged from 0.75 to 0.82.)

RESULTS AND DISCUSSION

Steps of Model Building and Refinement. An F_o electron density map based on the phases resulting from 4-fold map averaging (Fig. 1*A*) was of sufficient quality to unambiguously reveal the fold of most of the subunit, as well as to show many clear side chain densities. When placed in that map, the published AGA model was in good agreement for its most reliable and best defined secondary structure elements, although at several places it did significantly diverge from the map (Fig. 1*A*). The 10 secondary structure elements were extracted from the 331-residue published AGA model, changed to polyalanine, and idealized. Then other alanine residues were conservatively added, forming 4 additional secondary structure elements. This was used as the scaffold to build the rest of the EcA model. A stretch of sequence (5) in the C-terminal domain was correlated with electron density. Other alanine residues were replaced with residues chosen to fit the size and shape of the density in the map. The tetramer was generated in the asymmetric unit by applying 222 symmetry to the subunit model and was refined by using X-PLOR (23). After a few cycles of rebuilding, alternated with combination of the map-averaged phases and calculated model phases, and after further extension of the data to 2.8 Å, additional stretches of sequence could be identified in the map.

Even after all 326 amino acids were included, the density remained unclear for a loop between residues 11 and 24. Attempts to rebuild this region failed to produce correlation between the ($2F_o - F_c$) maps and the model. In the meantime, the structure of another asparaginase, isolated from *Erwinia chrysanthemi* (ErA), was solved in this laboratory using the EcA model as the MR probe. The density for the analogous loop region in the ErA maps was clearer and allowed for a definitive chain tracing. This segment was then excised from the ErA model and grafted onto the EcA model. After refinement, the quality of the maps was sufficiently enhanced to enable unambiguous tracing of this region of the EcA model.

A large, nonspherical peak of ($F_o - F_c$) difference density persisted near the base of the aforementioned loop after the tracing of the polypeptide chain was completed. This peak was found in the vicinity of Thr-12, the conserved amino acid that had been postulated to be in the active site (12, 16). It has been established that aspartate is an inhibitor of asparaginase and remains bound to EcA, although dialysis at high pH will remove most of it (26). It is likely that aspartate was present in the Elspar sample and remained there since the EcA

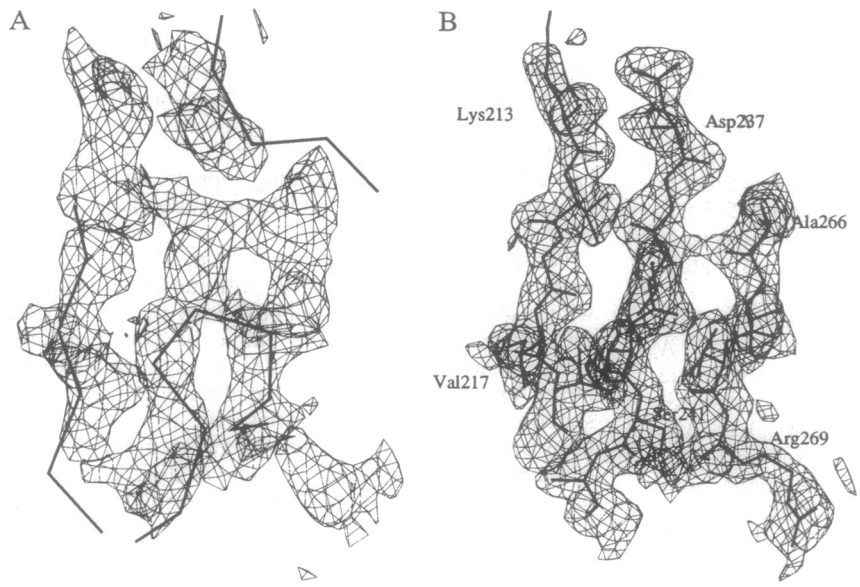

FIG. 1. β-Sheet region in the N-terminal domain. (*A*) The 3.0 Å averaged electron density map of EcA with the AGA model superimposed (thick lines), in an area with the poorest correlation between the map and the starting model. (*B*) The 2.3 Å ($2F_o - F_c$) electron density map with the refined EcA model superimposed (thick lines), emphasizing the correctness of the phasing of the 3.0 Å averaged electron density map shown in *A*.

crystals were grown at pH 5. In view of this and other structural evidence described later, aspartate was fit to this density.

The complete model was refined to convergence using X-PLOR (23). The final model consists of 1304 amino acids, 601 water molecules, and four aspartate ligands. The *R* factor is

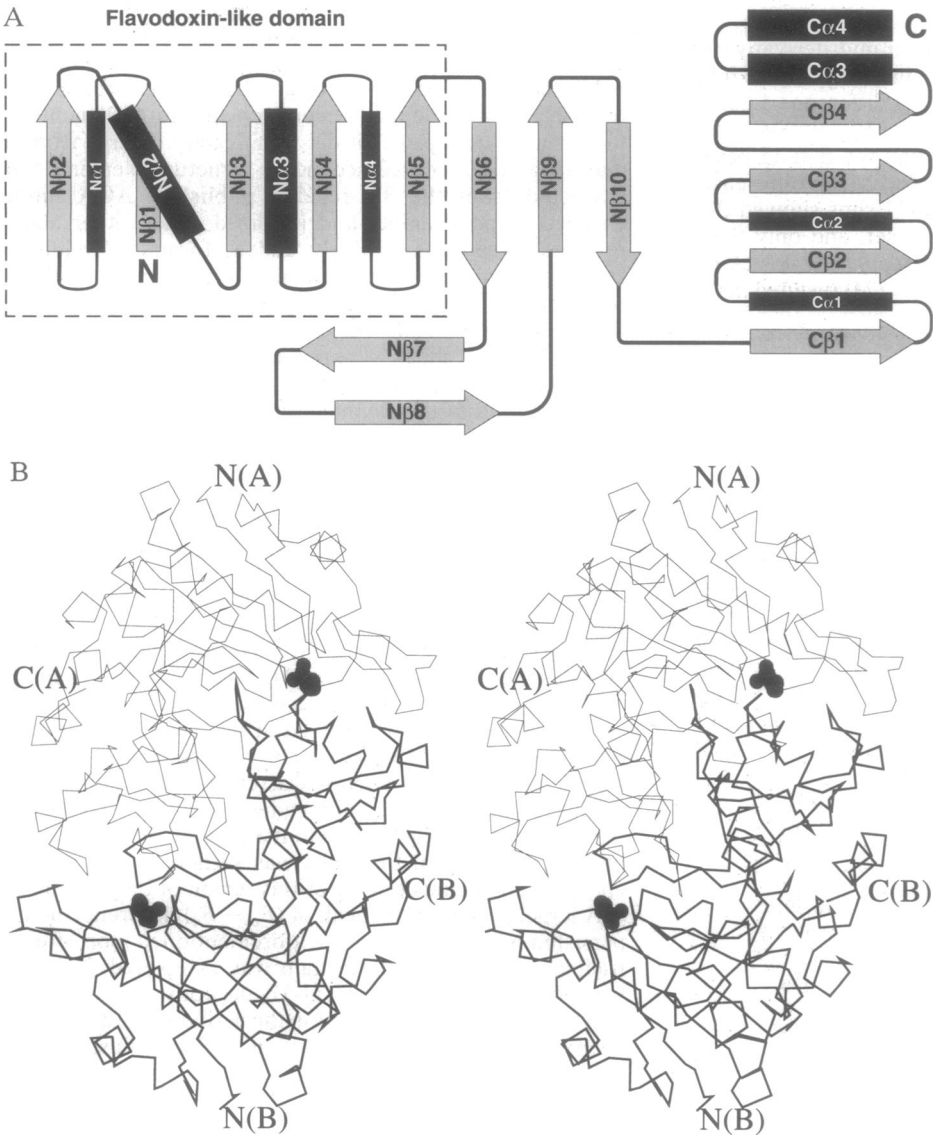

FIG. 2. (*A*) Topology of the EcA subunit with arrows representing β-strands, thin rectangles representing α-helices on one side of the sheet, and thick rectangles representing α-helices on the opposite side. The dashed box outlines the part of the structure that has a fold similar to that of flavodoxin. The active site is located at the topological switchpoint between the C-terminal ends of Nβ1 and Nβ3. The left-handed crossover occurs between Nβ4 and Nβ5. (*B*) Stereoview of an "intimate" dimer of EcA. The subunits of EcA are related by twofold noncrystallographic symmetry, with aspartate bound in each active site. The termini of the A and B subunits are labeled N(A) and C(A), and N(B) and C(B), respectively. The aspartate ligands are represented by space-filling models.

0.143 for 56,390 reflections between 10 and 2.3 Å, and the root-mean-square deviations from ideal bond and angle distances are 0.017 Å and 0.054 Å, respectively. In each subunit, all but one non-glycine residue lie in the "allowed" regions of the Ramachandran plot, the exception being Thr-198, the side chain of which makes hydrogen bonds stabilizing the linker region between the N- and C-terminal domains. The final electron density map is of very good quality (Fig. 1*B*).

Description of the Structure. The asparaginase subunit consists of two α/β domains (Fig. 2*A*) connected by the linking sequence 191–212. The N-terminal domain contains an eight-stranded mixed β-sheet. There is a topological switchpoint (27) between strands Nβ1 and Nβ3 where the C-terminal ends of those adjacent β-strands continue in opposite directions, folding into α-helices on either side of the sheet. This directional change of exit from the C-terminal ends of the β-strands creates a cleft characteristic of all parallel α/β structures that serves as a pocket utilized in ligand binding (27). The β-strand connectivity for the parallel part of the sheet is similar to that of flavodoxin (28) [$-1x$, $+2x$, $+1x$, $+1x$]. Even though helices in flavodoxin superimpose on the four N-terminal helices in EcA, they do so in different order. This is due to the occurrence of a left-handed crossover between strands Nβ4 and Nβ5. Left-handed crossovers, though rarely seen in protein structures, have been observed in the well-refined structures of subtilisin and acetylcholine esterase (29, 30).

The N-terminal domain of asparaginase contains four α-helices with Nα1 and Nα4 on one side of the β-sheet, exposed to solvent, and Nα2 and Nα3 on the opposite side, near the domain interface. Two antiparallel β-strands, Nβ7 and Nβ8, leave the main sheet and form a β-hairpin, which is positioned toward the interior of the tetramer and may play a role in subunit adhesion. A disulfide bridge [unique to EcA in the family of asparaginases (31)] between Cys-77 and Cys-105 is located on the surface at the N-terminal edge of the parallel part of the sheet, connecting the C-terminal end of Nα2 to the loop between Nα3 and Nβ4.

The smaller C-terminal domain (residues 213–326) consists of a four-stranded parallel β-sheet [$+1x$, $+1x$, $+1x$] and four α-helices. Helices Cα3 and Cα4 are on the interdomain side of the sheet while Cα1 and Cα2 are on the side distal to the domain interface.

The active, tetrameric form of asparaginase is composed of four identical subunits, A, B, C, and D, with approximate 222 symmetry. Of the six pairwise interactions among the subunits, those between A and B and between C and D are most extensive, forming two intimate pairs of subunits. In this respect, the tetramer is a dimer of identical intimate dimers (here called AB and CD) (Fig. 2*B*).

Active Sites. Locations for the four active sites of the tetramer have been identified on the basis of patches of electron density not belonging to the polypeptide chain, observed in the clefts formed by the topological switchpoints of each N-terminal domain. The size and shape of the electron density patch in each active site are indicative of an aspartate residue, which has been identified in purified asparaginase (26) (Fig. 3*A*). The active sites are located between subunits in the intimate dimers (Fig. 2*B*). Each dimer has two active sites, although only the tetramer has been reported to show activity. Each active site is made up primarily of residues from the N-terminal domain, with contacts from the C-terminal domain of the intimately bound subunit.

There are a number of polar side chains with atoms within 3.5 Å of the aspartate. The side chain oxygens of Gln-59, Asp-90, and Glu-283B, surrounding the α-amino group, presumably function to anchor the substrate/product. The α-carboxyl group has contacts with the main-chain nitrogens of Asp-90 and Ser-58 and with the O$^{\gamma}$ of Ser-58. The β-carboxyl group has contacts with the main-chain nitrogen of

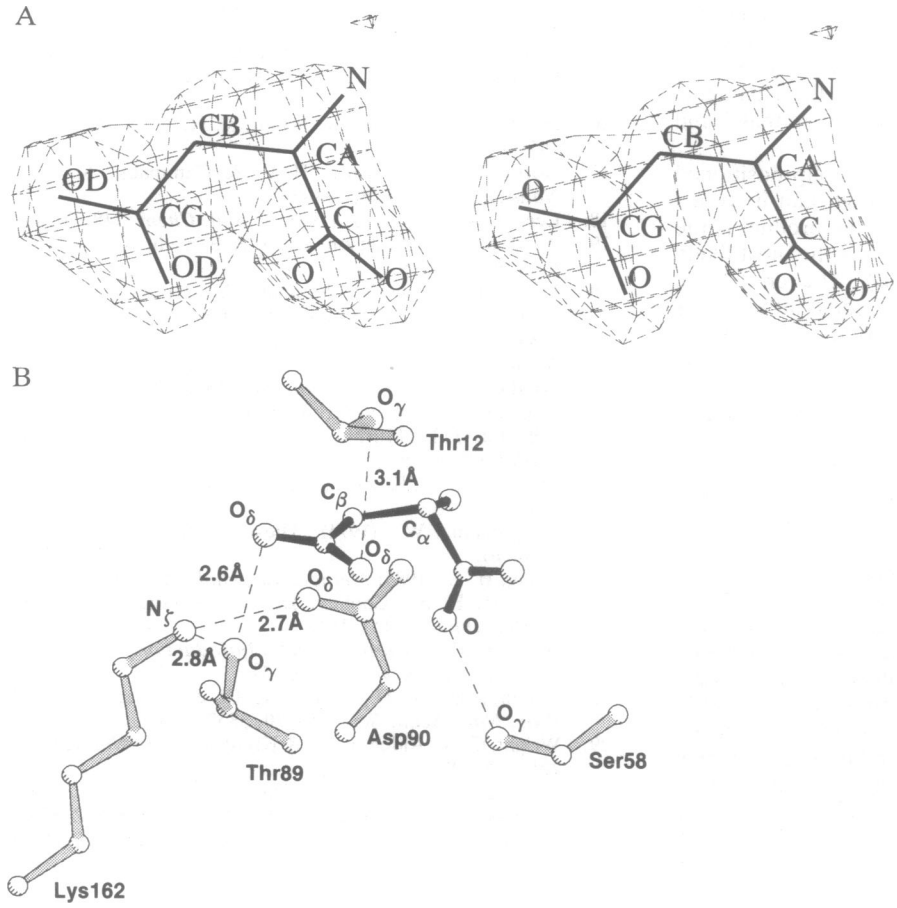

FIG. 3. (*A*) Stereoview of the density in the active site of subunit A with 2.3 Å ($2F_o - F_c$) electron density calculated after refinement, contoured at the 1σ level, with the bound aspartate model superimposed. The quality of the map is sufficient to unambiguously assign the orientation of the aspartate. (*B*) Active site of subunit A with side chains (shaded bonds) of the potentially nucleophilic residues <3.2 Å from the bound aspartate (solid bonds). Also shown are side chains that may influence the nucleophilicity of Thr-89.

Thr-89, the carbonyl oxygen of Ala-114, the O^{γ} of Thr-12, the O^{γ} of Thr-89, and a water molecule.

Some spherical electron density peaks found in the vicinity of the active site have been modeled as water molecules. Several water molecules are also seen beyond 3.5 Å from the modeled aspartate, lining a potential pathway to and/or from the active site. This is the only access to the active site of the enzyme in the conformation represented in this crystal form. One of the density peaks interpreted as a water molecule may alternatively correspond to an ammonium ion, the other product of the asparaginase reaction.

Ser-120, the residue that was modified by the substrate analog in EcA, is not near the active site as we have identified it. The distance from the aspartate in the active site to Ser-120 is ≈12.5 Å. This residue is positioned in the loop forming the left-handed crossover between strands Nβ4 and Nβ5, which is the site of contact for the tip of the flexible loop (residues 12–25) covering the active site. (The carbonyl oxygen of Ala-20 in the flexible loop hydrogen bonds to the main-chain nitrogen of Met-121.)

Enzymatic Mechanism. While details of the enzymatic mechanism are unclear, the reaction probably proceeds through a nucleophilic attack on the β-amide group of asparagine, leading to an acyl–enzyme intermediate (11, 26). On the basis of the proximity of their side chains to the aspartate ligand, Thr-12, Tyr-25, Ser-58, and Thr-89 could be potential nucleophiles. We studied the environment of these residues in search for neighboring residues that could influence their nucleophilic character. Although there is evidence that Thr-12 is directly involved in catalysis, the only residue within hydrogen-bonding distance is Tyr-25, which would not effect its nucleophilicity. The hydroxyl group of Tyr-25 itself is ≈4 Å from the bound aspartate, indicating that, if it were the nucleophilic residue, a conformational change in the main chain or a large shift in the position of the product would have occurred during catalysis.

The only polar side chain within hydrogen-bonding distance of Ser-58 is Thr-91, which would not be particularly effective in altering the nucleophilic character of Ser-58. Additionally, for Ser-58 to be the nucleophile, the asparagine substrate must assume the orientation opposite to that found for aspartate.

The bound aspartate has its β-carboxyl group positioned within hydrogen-bonding distance of Thr-89, and if we assume that the position and orientation of the product is the same as that of the substrate, then Thr-89 is the most likely candidate for the nucleophile (Fig. 3*B*). The only basic residue in the active site region, Lys-162, could influence its nucleophilic character. The interaction with the O^{δ} of Asp-90 could also influence the basicity of Lys-162. If Thr-89 is the nucleophile, the positions of Thr-12 and Tyr-25 are such that they could stabilize a tetrahedral intermediate. The α-amide nitrogen of the aspartate is positioned within hydrogen-bonding distance of Gln-59 and Asp-90, as well as Asn-248 and Glu-283, from the adjacent intimately bound subunit, potentially facilitating binding of the substrate or stabilization of the transition states.

The side chains extending into the compact catalytic cavity of asparaginase are acidic and polar and thus well suited to make hydrogen-bond interactions with the asparagine substrate or the aspartate product of the reaction. The distribution of charge is currently impossible to decipher and is likely to form an interdependent network. With an aspartate molecule found in the active site, it has been possible to speculate which of these residues are involved in binding and stabilizing the substrate and product. While there are several possibilities for the identity of the nucleophilic residue, we propose Thr-89 to be the most likely candidate based on the structural evidence. Further experiments, including diffraction studies of complexes of EcA with bound inhibitors and of mutants of EcA, will be needed to test the veracity of this hypothesis.

We are grateful to Irene Weber for supplying the coordinates of AGA, to Klaus Röhm for valuable discussion, and to Michael Gribskov and Maria Miller for the coordinates of loop 11–24 from ErA. We are indebted to Merck, Sharp and Dohme for the gift of Elspar and to the Biomedical Supercomputer Center, National Cancer Institute–Frederick Cancer Research and Development Center for an allocation of >400 central processing unit hours on their CRAY Y-MP computer. This work was supported in part by the National Cancer Institute, Department of Health and Human Services Contract N01-CO-74101 with the Advanced Biosciences Laboratory, by National Research Service Award Fellowship F32 CA 08909-02 to A.L.S., and by a grant from the Fondation pour la Recherche Thérapeutique to D.H.

1. Schwartz, J. H., Reeves, J. Y. & Broome, J. D. (1966) *Proc. Natl. Acad. Sci. USA* **56**, 1516–1519.
2. Cedar, H. & Schwartz, J. H. (1967) *J. Biol. Chem.* **242**, 3753–3755.
3. Cedar, H. & Schwartz, J. H. (1968) *J. Bacteriol.* **96**, 2043–2048.
4. Epp, O., Steigemann, W., Formanek, H. & Huber, R. (1971) *Eur. J. Biochem.* **20**, 432–437.
5. Jennings, M. P. & Beacham, I. R. (1990) *J. Bacteriol.* **172**, 1491–1498.
6. Hill, J. M., Roberts, J., Loeb, E., Khan, A., MacLellan, A. & Hill, R. W. (1967) *J. Am. Med. Assoc.* **202**, 116–122.
7. Beacham, I. & Jennings, M. (1990) *Today's Life Sci.* **2**, 40–42.
8. Rogers, K. S. (1989) *J. Am. Vet. Med. Assoc.* **194**, 1626–1630.
9. Haskell, C. M. & Canellos, G. P. (1969) *Biochem. Pharmacol.* **18**, 2578–2580.
10. Keefer, J. F., Moraga, D. A. & Schuster, S. M. (1985) *Biochem. Pharmacol.* **34**, 559–565.
11. Röhm, K. H. & Van Etten, R. L. (1986) *Arch. Biochem. Biophys.* **244**, 128–136.
12. Holcenberg, J. S., Ericsson, L. & Roberts, J. (1978) *Biochemistry* **17**, 411–417.
13. Peterson, R. G., Richards, F. F. & Handschumacher, R. E. (1977) *J. Biol. Chem.* **252**, 2072–2076.
14. Bagert, U. & Röhm, K. H. (1989) *Biochim. Biophys. Acta* **999**, 36–41.
15. Wehner, A., Harms, E., Jennings, M. P., Beacham, I. R., Derst, C., Bast, P. & Röhm, K. H. (1992) *Eur. J. Biochem.* **208**, 475–480.
16. Derst, C., Henseling, J. & Röhm, K. H. (1992) *Protein Eng.* **5**, 785–789.
17. North, A. C. T., Wade, H. E. & Cammack, K. A. (1968) *Nature (London)* **224**, 594–595.
18. Lee, B. & Yang, H. J. (1973) *J. Biol. Chem.* **248**, 7620–7623.
19. Wlodawer, A., Hodgson, K. O. & Bensch, K. (1975) *J. Mol. Biol.* **99**, 295–299.
20. Mitsui, Y., Satow, Y., Watanabe, Y., Hirono, S., Yonei, M., Urata, Y., Torii, K. & Iitaka, Y. (1978) *Acta Crystallogr. Sect. A* **34**, S60 (abstr.).
21. Ammon, H. L., Murphy, K. C., Chandrasekhar, K. & Wlodawer, A. (1985) *J. Mol. Biol.* **184**, 179–181.
22. Ammon, H. L., Weber, I. T., Wlodawer, A., Harrison, R. W., Gilliland, G. L., Murphy, K. C., Sjölin, L. & Roberts, J. (1988) *J. Biol. Chem.* **263**, 150–156.
23. Brünger, A. T., Kuriyan, J. & Karplus, M. (1987) *Science* **235**, 458–460.
24. Steigemann, W. (1974) Thesis (Technische Universität, Munich).
25. Wang, B. C. (1985) *Methods Enzymol.* **115**, 90–112.
26. Jayaram, H. N., Cooney, D. A. & Huang, C. Y. (1968) *J. Enzyme Inhib.* **1**, 151–161.
27. Brändén, C. & Tooze, J. (1991) *Introduction to Protein Structure* (Garland, New York), p. 51.
28. Watenpaugh, K. D., Sieker, L. C. & Jensen, L. H. (1973) *Proc. Natl. Acad. Sci. USA* **70**, 3857–3860.
29. Wright, C. S., Alden, R. A. & Kraut, J. (1969) *Nature (London)* **221**, 235–242.
30. Sussman, J. L., Harel, M., Frolow, F., Oefner, C., Goldman, A., Toker, L. & Silman, I. (1991) *Science* **253**, 872–878.
31. Greenquist, A. C. & Wriston, J. C., Jr. (1972) *Arch. Biochem. Biophys.* **152**, 280–286.